

Non-Linear Shallow Water Equations numerical integration on curvilinear boundary-conforming grids

GIOVANNI CANNATA
Dip. di Ingegneria Civile,
Edile e Ambientale
Sapienza University of
Rome
Via Eudossiana 18, 00184
Rome
ITALY
giovanni.cannata@uniroma1
.it

FRANCESCO
LASAPONARA
Dip. di Ingegneria Civile,
Edile e Ambientale
Sapienza University of
Rome
Via Eudossiana 18, 00184
Rome
ITALY
francesco.lasaponara@unirom
a1.it

FRANCESCO
GALLERANO
Dip. di Ingegneria Civile,
Edile e Ambientale
Sapienza University of
Rome
Via Eudossiana 18, 00184
Rome
ITALY
francesco.gallerano@unirom
a1.it

Abstract: - An Upwind Weighted Essentially Non-Oscillatory scheme for the solution of the Shallow Water Equations on generalized curvilinear coordinate systems is proposed. The Shallow Water Equations are expressed in a contravariant formulation in which Christoffel symbols are avoided. The equations are solved by using a high-resolution finite-volume method incorporated with an exact Riemann Solver. A procedure developed in order to correct errors related to the difficulties of numerically satisfying the metric identities on generalized boundary-conforming grids is presented; this procedure allows the numerical scheme to satisfy the freestream preservation property on highly-distorted grids. The capacity of the proposed model is verified against test cases present in literature. The results obtained are compared with analytical solutions and alternative numerical solutions.

Key-Words: - 2D Shallow Water Equations, Upwind WENO scheme, Contravariant formulation, Christoffel Symbols, Freestream preservation.

1 Introduction

Many authors [10,26,39] solve Shallow Water Equations by using high-resolution methods for hyperbolic systems of conservation laws. In this context Weighted Essentially Non-Oscillatory (WENO) schemes [24,28] are very efficient tools. Two classes of methods can be distinguished: Upwind and Central schemes.

Upwind schemes are physically based and require extensive use of eigensystems: the calculation of cell averages needs information on characteristics at the interfaces of spatial cells. In most cases the solution of a Riemann problem is involved in tracing the characteristic fans. Rossmannith et al. [33] adopted a Roe-type approximate Riemann solver for hyperbolic system in a general curved manifold: the equations are solved in the coordinate basis defined by the numerical grid and all one-dimensional Riemann problems are solved in a locally valid orthonormal basis. Even though approximate Riemann solvers can give good results, some researchers [3,32,43]

opt for the so-called exact solver through some numerical iterative schemes.

In order to simulate flows over computational domains characterized by a complex boundary two strategies can be followed. The first strategy is represented by the possibility of using unstructured grids [2,7,8,9,12,13,14,20,21,29,37]. The second strategy is based on the numerical integration of the motion equations on a generalized curvilinear boundary conforming grid [15,16,17,18,19,34]. In generalized curvilinear coordinates, contravariant components are vector components defined on a basis which is locally normal to the curvilinear coordinates. This strategy has been widely used in numerical simulations of shallow water on the surface of a sphere, as well as relativistic hydrodynamics [11,30].

In numerical solutions of motion equations in contravariant formulation two contradictions appear. The first contradiction is related to the presence of Christoffel symbols in motion equations. It is well known [47] that numerical methods for the solution of the conservation laws in which the convective

terms are expressed in non-conservative form do not guarantee the convergence to weak solutions. Consequently in the integrations of the conservation laws in whose solutions shocks are present, convective terms must be expressed in conservative form. In the contravariant formulation of motion equations, covariant derivatives give rise to Christoffel symbols. These terms are extra source terms. They come in with the variability of base vectors and do not permit the definition of convective terms in a conservation form. Consequently the contravariant Shallow Water Equations, numerically integrated on generalized boundary conforming curvilinear grids for the simulation of flows in which shocks are present, must be free of Christoffel symbols. Furthermore, it is well known that in numerical methods in which numerical approximations of derivatives of uniform physical quantities do not vanish, freestream conditions are not preserved. In other words, the freestream preservation properties of a scheme are achieved when a uniform field is not affected by mesh irregularities. Numerical discretizations of the Christoffel symbols introduce computation errors related to mesh non-uniformities: solutions are affected by these non-uniformities. As a consequence numerical discretization of the above mentioned symbols can reduce the numerical accuracy and can corrupt the preservation of freestream conditions. Wesseling et al. [44], Xu and Zhang [46] and Yang et al. [47] avoid the Christoffel symbols and ensure the strong conservation properties by dotting the strongly conservative motion equations in vector form by the contravariant base vector after the discretizations.

The second contradiction is related to the difficulty of exactly numerically satisfying the metric identities. A well known geometric identity [41] is given by the condition that a cell is closed. In a curvilinear system of reference the aforementioned condition becomes the metric identity. If numerical approximations of the metric coefficients do not exactly satisfy the above mentioned identity, numerical approximations of derivatives of uniform physical quantities do not vanish and freestream conditions are not preserved. Many authors [4,42] solve the problem by constructing meshes in which metric identities can be numerically satisfied through careful attention to the evaluation of the metric coefficients. Nonomura et al. [31] state that in schemes, as WENO schemes, in which unsymmetrical high-order operators are involved, the above mentioned procedures (based on the careful evaluation of the metric coefficients) are not able to satisfy numerically the metric identities.

The original contribution of this work is the definition of a new Upwind Weighted Essentially Non-Oscillatory scheme for the solution of the Shallow Water Equations expressed directly in contravariant formulation. The Upwind WENO scheme needs a flux calculation at the cell interfaces. These fluxes are calculated by means of the solution of a Riemann problem. An Exact Riemann Solver is used in this work. In accordance with the procedure proposed by Rossmannith et al. [33], all necessary Riemann problems are solved in a locally valid orthonormal basis. This orthonormalization allows one to solve Cartesian Riemann problems that are devoid of geometric terms. Following the conceptual line proposed in [16], in this paper a formal integral expression of the Shallow Water Equations in contravariant formulation is presented. In order to avoid Christoffel symbols, the depth-integrated motion equations (in contravariant form) are integrated on an arbitrary surface and are resolved in the direction identified by a constant parallel vector field. In this way we present an integral form of the contravariant Shallow Water Equations in which Christoffel symbols are avoided. A procedure developed in order to correct errors related to the difficulties of numerically satisfying the metric identities on generalized boundary-conforming grids is presented; this procedure allows the numerical scheme to satisfy the freestream preservation property on highly-distorted grids. The model is verified against several benchmark tests, and the results are compared with theoretical and alternative numerical solutions.

2 The integral form of contravariant Shallow Water Equations

We define the water depth as h and the depth-averaged velocity vector as \vec{u} , whose components are defined in the Cartesian system of reference. Let be $\vec{v} = h\vec{u}$. The Shallow Water Equations are written directly in the contravariant formulation in a two-dimensional curvilinear coordinate system.

In order to introduce the notation to be used, we consider a transformation $x^l = x^l(\xi^1, \xi^2)$ from the Cartesian coordinates \vec{x} to the curvilinear coordinates $\vec{\xi}$ (note that superscripts indicate components and not powers in the present notation). Let $\vec{g}_{(l)} = \partial\vec{x}/\partial\xi^l$ the covariant base vectors and $\vec{g}^{(l)} = \partial\xi^l/\partial\vec{x}$ the contravariant base vectors. The

metric tensor and its inverse are defined by $g_{lm} = \bar{g}_{(l)} \cdot \bar{g}_{(m)}$ and $g^{lm} = \bar{g}^{(l)} \cdot \bar{g}^{(m)}$ ($l, m = 1, 2$).

The Jacobian of the transformation is given by $\sqrt{g} = \sqrt{\det(g_{lm})}$. The transformation relationship between vector \vec{b} in the Cartesian coordinate system and its contravariant and covariant components, b^l and b_l , in the curvilinear coordinate system are given by [40]

$$\begin{aligned} b^l &= \bar{g}^{(l)} \cdot \vec{b}; & b_l &= \bar{g}_{(l)} \cdot \vec{b}; \\ \vec{b} &= b^l \bar{g}_{(l)}; & \vec{b} &= b_l \bar{g}^{(l)} \end{aligned} \quad (1)$$

The same relationship also applies to other vectors. In the following equations, a comma with an index in a subscript denotes covariant differentiation. The covariant derivative is defined as $b^{l,m} = \partial b^l / \partial \xi^m + \Gamma_{mk}^l b^k$ where Γ_{mk}^l is the Christoffel symbol that is given by $\Gamma_{mk}^l = \bar{g}^{(l)} \cdot \partial \bar{g}_{(k)} / \partial \xi^m$ [1].

The integral form of the contravariant continuity equations is given by:

$$\iint_{\Delta A} \frac{\partial h}{\partial t} dA + \int_L r^m n_m dL = 0 \quad (2)$$

where ΔA is an arbitrary surface elements, L the contour line. The second integral of Eq. (2) has been transformed by Green's theorem.

From a general point of view, in order to express the momentum conservation law in integral form, the rate of change of momentum of a material volume and the total net force must be projected onto a physical direction. The direction in space of a given coordinate line is changing, in contrast with the Cartesian case. Thus, the volume integral of the projection of motion equations onto a curvilinear coordinate line has no physical meaning since it does not represent the volume integral of the projection of the aforementioned equations onto a physical direction [1]. We take a constant parallel vector field and equate the rate of change of momentum of a material volume to the total net force in this direction. We choose, as parallel vector field, the one which is normal to the coordinate line on which the ξ^l coordinate is constant at point $P_0 \in \Delta A$. The coordinate values of P_0 are ξ_0^1 and ξ_0^2 . The contravariant base vector at point P_0 , $\bar{g}^{(l)}(\xi_0^1, \xi_0^2)$, which is normal to the coordinate line on which ξ^l is constant, is used in this work in order to identify the parallel vector field.

Let $\lambda_k(\xi^1 \xi^2)$ be the covariant component of $\vec{g}^{(l)}(\xi_0^1, \xi_0^2)$, given by

$$\lambda_k(\xi^1 \xi^2) = \bar{g}^{(l)}(\xi_0^1, \xi_0^2) \cdot \bar{g}_{(k)}(\xi^1, \xi^2) \quad (3)$$

For the sake of brevity, we indicate $\vec{g}^{(l)} = \bar{g}^{(l)}(\xi_0^1, \xi_0^2)$ and $\bar{g}_{(k)} = \bar{g}_{(k)}(\xi^1, \xi^2)$. We integrate over an arbitrary surface element of area ΔA and resolve in the direction λ_k the rate of change of the depth-integrated momentum (per unit mass) and the depth-integrated force (per unit mass). Consequently we get:

$$\begin{aligned} & \iint_{\Delta A} \frac{\partial r^k}{\partial t} \lambda_k dA + \\ & \iint_{\Delta A} \left(\frac{r^k r^m}{h} + G g^{km} \frac{h^2}{2} \right)_{,m} \lambda_k dA = \\ & - \iint_{\Delta A} [G h g^{km} H_{,m} + R^k] \lambda_k dA \end{aligned} \quad (4)$$

Since the vector field is constant and parallel, $\lambda_{k,m} = 0$. The second integral on the left hand side of Eq. (4) can be transformed by Green's theorem; Eq. (4) becomes

$$\begin{aligned} & \iint_{\Delta A} \frac{\partial r^k}{\partial t} \lambda_k dA + \\ & \int_{\Delta L} \left(\frac{r^k r^m}{h} + G g^{km} \frac{h^2}{2} \right) n_m \lambda_k dL = \\ & - \iint_{\Delta A} [G h g^{km} H_{,m} + R^k] \lambda_k dA \end{aligned} \quad (5)$$

By using Eq. (3) and by recalling $\bar{g}^{(l)} \cdot \bar{g}_{(k)} = \delta_{lk}$ we get

$$\begin{aligned} & \iint_{\Delta A} \bar{g}^{(l)} \cdot \bar{g}_{(k)} \frac{\partial r^k}{\partial t} dA + \\ & \int_{\Delta L} \left(\bar{g}^{(l)} \cdot \bar{g}_{(k)} \frac{r^k r^m}{h} + \bar{g}^{(l)} \cdot \bar{g}^{(m)} G \frac{h^2}{2} \right) n_m dL = \\ & - \iint_{\Delta A} \bar{g}^{(l)} \cdot \bar{g}_{(k)} [G h g^{km} H_{,m} + R^k] dA \end{aligned} \quad (6)$$

Eq. (2) and (6) represent the integral expressions of the Shallow Water Equations in contravariant formulation in which Christoffel symbols are absent.

Let us introduce a restrictive condition on the surface element of area ΔA : in the following the surface element of area ΔA must be considered as a surface element which is bounded by four curves lying on the coordinate lines. Since $dA =$

$\sqrt{g}d\xi^1d\xi^2$ and by indicating with \tilde{h} the averaged value of h over the surface element of area ΔA , given by $\tilde{h} = \frac{1}{\Delta A} \iint_{\Delta A} h\sqrt{g}d\xi^1d\xi^2$ eq. (2) is transformed in

$$-\frac{1}{\Delta A} \sum_{\alpha=1}^2 \left[\int_{\Delta\xi^{\alpha+}} r^\alpha \sqrt{g}d\xi^\beta - \int_{\Delta\xi^{\alpha-}} r^\alpha \sqrt{g}d\xi^\beta \right] \frac{\partial \tilde{h}}{\partial t} = \quad (7)$$

where $\Delta\xi^{\alpha+}$ and $\Delta\xi^{\alpha-}$ indicate the segments of the contour line on which ξ^α is constant and which are located at the larger and smaller value of ξ^α , respectively. Here the indexes α and β are cyclic.

Let us define \tilde{r}^l as

$$\tilde{r}^l = \frac{1}{\Delta A} \iint_{\Delta A} \vec{g}^{(l)} \cdot \vec{g}_{(k)} r^k \sqrt{g}d\xi^1d\xi^2 \quad (8)$$

By dividing Eq. (6) by ΔA , by using Eq. (8) and by decomposing in three parts the source term related to the bottom slope, Eq. (6) becomes:

$$\begin{aligned} \frac{\partial \tilde{r}^l}{\partial t} = \frac{1}{\Delta A} \left\{ - \sum_{\alpha=1}^2 \left[\int_{\Delta\xi^{\alpha+}} \left(\vec{g}^{(l)} \cdot \vec{g}_{(k)} \frac{r^k r^\alpha}{h} + \right. \right. \right. \\ \left. \left. \vec{g}^{(l)} \cdot \vec{g}^{(\alpha)} G \frac{h^2}{2} \right) \sqrt{g}d\xi^\beta - \int_{\Delta\xi^{\alpha-}} \left(\vec{g}^{(l)} \cdot \vec{g}_{(k)} \frac{r^k r^\alpha}{h} + \vec{g}^{(l)} \cdot \vec{g}^{(\alpha)} G \frac{h^2}{2} \right) \sqrt{g}d\xi^\beta \right] - \\ \iint_{\Delta A} \vec{g}^{(l)} \cdot \vec{g}_{(k)} [G(\eta - \tilde{\eta})g^{km}H_{,m} + \\ R^k] \sqrt{g}d\xi^1d\xi^2 - G\tilde{\eta} \sum_{\alpha=1}^2 \left[\int_{\Delta\xi^{\alpha+}} \vec{g}^{(l)} \cdot \vec{g}^{(\alpha)} H \sqrt{g}d\xi^\beta - \int_{\Delta\xi^{\alpha-}} \vec{g}^{(l)} \cdot \vec{g}^{(\alpha)} H \sqrt{g}d\xi^\beta \right] + \\ \left. \frac{G}{2} \sum_{\alpha=1}^2 \left[\int_{\Delta\xi^{\alpha+}} \vec{g}^{(l)} \cdot \vec{g}^{(\alpha)} H^2 \sqrt{g}d\xi^\beta - \int_{\Delta\xi^{\alpha-}} \vec{g}^{(l)} \cdot \vec{g}^{(\alpha)} H^2 \sqrt{g}d\xi^\beta \right] \right\} \quad (9) \end{aligned}$$

in which η is the free surface elevation and $\tilde{\eta}$ represents the averaged value of η on the surface element ΔA . The left hand side of Eq. (9) represents

the surface-average of the time derivative of the l contravariant component of the \vec{v} vector (expressed as a function of the contravariant base vector $\vec{g}^{(l)}$ defined in (ξ_0^1, ξ_0^2)). The last three terms on the right-hand side of Eq. (9) are obtained by decomposing the source term related to the bottom slope on the right-hand side of Eq. (6), according to the conceptual line proposed by Xing and Shu [45], in order to realize a numerical scheme that satisfies the C-property for quiescent flow over non-flat bottom. It must be noted that in Eq. (6) and in Eq. (9) Christoffel symbols are absent.

3 Metric identities and freestream preservation

Cai and Ladeinde [4] state that one of the main problems related to the solution of motion equations in generalized curvilinear coordinates is the difficulty of exactly numerically satisfying the metric identities; the failure to numerically satisfy the metric identities causes numerical instabilities in the solution. In the case in which metric identities are not exactly satisfied, freestream conditions are not preserved and, consequently, the fidelity of high-order approaches can be catastrophically destroyed [42]. In this section we present a procedure developed in order to correct errors related to the difficulties of numerically satisfying the metric identities on generalized boundary conforming grids.

A well known geometric identity [41] is given by the condition that a cell is closed. This condition is expressed by:

$$\oint_L \vec{n} dL = 0 \quad (10)$$

where \vec{n} represents the vector which is normal to the contour L of the calculation cell. In a curvilinear system of reference the condition (10) becomes the following metric identity in integral form

$$\sum_{\alpha=1}^2 \left[\int_{\Delta\xi^{\alpha+}} \vec{g}^{(\alpha)} \sqrt{g}d\xi^\beta - \int_{\Delta\xi^{\alpha-}} \vec{g}^{(\alpha)} \sqrt{g}d\xi^\beta \right] = 0 \quad (11)$$

Here the indexes (α, β) are cyclic. By dividing Eq. (11) for the area of the calculation cell $\Delta A = \iint \sqrt{g}d\xi^1d\xi^2$, and by applying the limit as ΔA

tends to zero, the following metric identity in differential form is obtained

$$\frac{\partial \vec{g}^{(\alpha)} \sqrt{g}}{\partial \xi^\alpha} = 0 \quad (12)$$

The most important effect produced on numerical solutions by the high levels of irregularity of the mesh is related to the metric identities. In order to emphasize the role of the metric identities in the failure of freestream preservation properties of a scheme, it is necessary to underline that in the summations of the integrals on the right-hand side of Eqs. (9) and (7), the terms on the left-hand side of the metric identities (11) and (12) are implicitly involved. In order to clarify the aforementioned involvement, we limit our analysis to the first term on the left-hand side of Eq. (9). The abovementioned term can be expressed as:

$$\begin{aligned} & \frac{1}{\Delta A} \sum_{\alpha=1}^2 \left[\int_{\Delta \xi^{\alpha+}} \left(\vec{g}^{(l)} \cdot \vec{g}^{(k)} \frac{r^k r^\alpha}{h} + \vec{g}^{(l)} \cdot \right. \right. \\ & \left. \left. \vec{g}^{(\alpha)} G \frac{h^2}{2} \right) \sqrt{g} d\xi^\beta - \int_{\Delta \xi^{\alpha-}} \left(\vec{g}^{(l)} \cdot \right. \right. \\ & \left. \left. \vec{g}^{(k)} \frac{r^k r^\alpha}{h} + \vec{g}^{(l)} \cdot \vec{g}^{(\alpha)} G \frac{h^2}{2} \right) \sqrt{g} d\xi^\beta \right] = \\ & \frac{1}{\Delta A} \iint_{\Delta A} \frac{\partial}{\partial \xi^\alpha} \left[\left(\vec{g}^{(l)} \cdot \vec{g}^{(k)} \frac{r^k r^\alpha}{h} + \vec{g}^{(l)} \cdot \right. \right. \\ & \left. \left. \vec{g}^{(\alpha)} G \frac{h^2}{2} \right) \sqrt{g} \right] d\xi^1 d\xi^2 \quad (13) \end{aligned}$$

Recalling that $r^\alpha = \vec{v} \cdot \vec{g}^{(\alpha)}$,

$$\begin{aligned} & \frac{1}{\Delta A} \iint_{\Delta A} \frac{\partial}{\partial \xi^\alpha} \left[\left(\vec{g}^{(l)} \cdot \vec{g}^{(k)} \frac{r^k r^\alpha}{h} + \vec{g}^{(l)} \cdot \right. \right. \\ & \left. \left. \vec{g}^{(\alpha)} G \frac{h^2}{2} \right) \sqrt{g} \right] d\xi^1 d\xi^2 = \frac{1}{\Delta A} \iint_{\Delta A} \vec{g}^{(\alpha)} \sqrt{g} \cdot \\ & \frac{\partial}{\partial \xi^\alpha} \left[\left(\vec{g}^{(l)} \cdot \vec{g}^{(k)} \frac{\vec{v} r^k}{h} + \vec{g}^{(l)} G \frac{h^2}{2} \right) \right] d\xi^1 d\xi^2 + \\ & \frac{1}{\Delta A} \iint_{\Delta A} \left[\left(\vec{g}^{(l)} \cdot \vec{g}^{(k)} \frac{\vec{v} r^k}{h} + \vec{g}^{(l)} G \frac{h^2}{2} \right) \right] \cdot \\ & \frac{\partial \vec{g}^{(\alpha)} \sqrt{g}}{\partial \xi^\alpha} d\xi^1 d\xi^2 \quad (14) \end{aligned}$$

The second term on the right-hand side of Eq. (14) is null, owing to the metric identity (12). Eqs. (13) and (14) show that the left-hand side of Eq. (13) implicitly contains the left-hand side of the metric identity (12); therefore, the numerical approximation of the left-hand side of Eq. (13) implicitly involves the numerical approximation of the left-hand side of Eq. (12). Consequently the

errors due to the numerical approximation of the metric terms in the discretization of the left-hand side of Eq. (13) prevent the satisfaction of the metric identity (12). The numerical approximation of the second term on the right-hand side of Eq. (14) represents a measure of the error produced by the failure of the satisfaction of the metric identity and has the effect of extra source terms. Following an analogous procedure, it can be shown that the following term

$$\frac{1}{\Delta A} \iint_{\Delta A} \vec{v} \cdot \frac{\partial \vec{g}^{(\alpha)} \sqrt{g}}{\partial \xi^\alpha} d\xi^1 d\xi^2 \quad (15)$$

is implicitly contained in the first term on the right-hand side of Eq. (7).

In the case of a uniform field, the error due to the failure in the satisfaction of the metric identity is evident: the second term on the right-hand side of Eq. (14) and the term (15) do not vanish and consequently a uniform field does not remain uniform and freestream conditions are not preserved. Nonomura et al. [31] state that in schemes, such as WENO schemes, in which unsymmetric high-order operators are involved, procedures based on the careful evaluation of the metric coefficients are not able to numerically satisfy the metric identities. In this work, in order to correct the effects produced by the spurious source terms related to the difficulties of numerically satisfying the metric identities, the numerical approximation of

$$\begin{aligned} & \frac{\vec{v}}{\Delta A} \cdot \\ & \sum_{\alpha=1}^2 \left[\int_{\Delta \xi^{\alpha+}} \vec{g}^{(\alpha)} \sqrt{g} d\xi^\beta - \int_{\Delta \xi^{\alpha-}} \vec{g}^{(\alpha)} \sqrt{g} d\xi^\beta \right] \quad (16) \end{aligned}$$

$$\begin{aligned} & \frac{\left(r^{\frac{\vec{v}}{h}} + \vec{g}^{(l)} G \frac{h^2}{2} \right)}{\Delta A} \cdot \sum_{\alpha=1}^2 \left[\int_{\Delta \xi^{\alpha+}} \vec{g}^{(\alpha)} \sqrt{g} d\xi^\beta - \right. \\ & \left. \int_{\Delta \xi^{\alpha-}} \vec{g}^{(\alpha)} \sqrt{g} d\xi^\beta \right] \quad (17) \end{aligned}$$

are introduced on the right-hand side of Eqs. (7) and (9), respectively, where \vec{v} represents the averaged value of \vec{v} over the surface element of area ΔA . The numerical approximations of the aforementioned terms are performed by the same weights used in the WENO approximations, respectively, of the first terms on the left hand side of Eqs. (7) and (9). In this way we eliminate the errors produced by the

difficulties of exactly satisfying the metric identities and then we achieve the freestream preservation.

4 The Upwind WENO scheme

In this section we present the procedure for the numerical integration of Eqs. (7) and (9).

The numerical integration of Eqs. (7) and (9) is performed by an Upwind WENO scheme. The discretization of the computational domain is based on a grid defined by the coordinate lines ξ^1 and ξ^2 and by the points of coordinates $\xi^1 = i\Delta\xi^1$ and $\xi^2 = j\Delta\xi^2$, which represent the centers of the calculation cells $I_{i,j} = (\xi_{i-1/2}^1, \xi_{i+1/2}^1) \times (\xi_{j-1/2}^2, \xi_{j+1/2}^2)$. t^n is the time level of the known variables, while t^{n+1} is the time level of the unknown variables. Let us indicate with $\mathbf{L}(r^1, r^2, t)$ the right-hand side of Eq. (7) and with $\mathbf{D}(h, r^1, r^2, t)$ the right-hand side of Eq. (9).

By integrating Eqs. (7) and (9) over (t^n, t^{n+1}) we get:

$$\tilde{h}_{i,j}^{(n+1)} = \tilde{h}_{i,j}^{(n)} - \frac{1}{\Delta A} \int_{t^n}^{t^{n+1}} \mathbf{L}(r^1, r^2, t) dt \quad (18)$$

$$\tilde{r}_{i,j}^{l(n+1)} = \tilde{r}_{i,j}^{l(n)} - \frac{1}{\Delta A} \int_{t^n}^{t^{n+1}} \mathbf{D}(h, r^1, r^2, t) dt \quad (19)$$

Eqs. (18) and (19) represent the advancing from time level t^n to time level t^{n+1} of the variables $\tilde{h}_{i,j}$ and $\tilde{r}_{i,j}$. The state of the system is known at the center of the calculation cell and it is defined by the cell-averaged values $\tilde{h}_{i,j}$ and $\tilde{r}_{i,j}$.

In this work the five stage fourth order accurate Strong Stability Preserving Runge-Kutta (SSPRK) method [35] is used in order to achieve the time integration of Eqs. (18) and (19). In compact form the SSPRK method is described by the following equations:

$$\tilde{h}_{i,j}^{(0)} = \tilde{h}_{i,j}^{(n)} ; \quad \tilde{r}_{i,j}^{l(0)} = \tilde{r}_{i,j}^{l(n)} \quad (20)$$

$$\tilde{h}_{i,j}^{(p)} = \sum_{q=0}^{p-1} \left\{ \Omega_{pq} h_{i,j}^{(q)} + \Delta t \varphi_{pq} [\mathbf{L}(r^1(q), r^2(q), t^n + d_q \Delta t)] \right\} \quad (21)$$

$$\tilde{r}_{i,j}^{l(p)} = \sum_{q=0}^{p-1} \left\{ \Omega_{pq} r_{i,j}^{l(q)} + \Delta t \varphi_{pq} [\mathbf{D}(h^{(q)}, r^{1(q)}, r^{2(q)}, t^n + d_q \Delta t)] \right\} \quad (22)$$

$$\tilde{h}_{i,j}^{(n+1)} = \tilde{h}_{i,j}^{(5)} ; \quad \tilde{r}_{i,j}^{l(n+1)} = \tilde{r}_{i,j}^{l(5)} \quad (23)$$

with $p=1, \dots, 5$. See Spiteri and Ruuth [35] for the values of the coefficients Ω_{pq} , φ_{pq} and d_q .

For the calculation of terms $\mathbf{L}(r^1, r^2, t)$ and $\mathbf{D}(h, r^1, r^2, t)$, the numerical approximation of integrals on the right-hand side of Eqs. (7) and (9) is required. The aforementioned calculation is based on the following sequence:

- WENO reconstructions, from cell averaged values, of the point values of the unknown variables at the center of the contour segments which define the calculation cells. At the center of the contour segment which is in common with two adjacent cells, twopoint values of the unknown variables are reconstructed by means of two WENO reconstructions defined on the two adjacent cells.
- Advancing in time of the point values of the unknown variables at the center of the contour segments by means of the so-called exact solution of a local Riemann problem, with initial data given by the pair of point-values computed by two WENO reconstructions defined on the two adjacent cells.
- Calculation of the spatial integrals which define $\mathbf{L}(r^1, r^2, t)$ and $\mathbf{D}(h, r^1, r^2, t)$.

4.1 Advancing time of point values at cell interface

At the center of the segments which define the calculation cells, two point values of the unknown variables are reconstructed, by means of two WENO reconstructions defined on the two adjacent cells. For example, at the center of the segment which is the interface between cell $I_{i,j}$ and cell $I_{i-1,j}$, WENO reconstructions defined on the aforementioned cells lead to the evaluation of the variables $h_{i-1/2,j}^{(n)-}, h_{i-1/2,j}^{(n)+}, r_{i-1/2,j}^{l(n)-}, r_{i-1/2,j}^{l(n)+}$. The advancing in time of the aforementioned variables is carried out by means of the so-called exact solution of an apposite Riemann problem, with initial data given by the pair of point-values computed by two WENO reconstructions. Generally speaking, the Riemann problem in a curvilinear coordinate system is more difficult to solve than the Riemann problem for the

same set of hyperbolic equations in an orthonormal frame. Following the approach suggested by Rossmannith et al. [33] we solve all Riemann problems in a locally valid orthonormal basis.

We define the normal and tangential to the coordinate line ξ^β depth-integrated velocity components as $q^{\alpha(n)}$ and $\tau^{\alpha(n)}$, respectively. Here the indexes α and β are cyclic. As $\vec{g}^{(\alpha)}/\sqrt{g^{\alpha\alpha}}$ and $\vec{g}_{(\beta)}/\sqrt{g_{\beta\beta}}$ (no sum on the repeated indexes α and β) are the unit vectors which are normal and tangential, respectively, to the coordinate line ξ^β and recalling relation (1), the following transformation relations are obtained

$$q^{\alpha(n)} = \frac{r^{\alpha(n)}}{\sqrt{g^{\alpha\alpha}}} \quad (24)$$

$$\tau^{\alpha(n)} = r^{\alpha(n)} \frac{g_{\alpha\beta}}{\sqrt{g_{\beta\beta}}} + r^{\beta(n)} \sqrt{g_{\beta\beta}} \quad (25)$$

(no sum on the repeated indexes α and β). For example, in the point of coordinates $(\xi_{i-1/2}^1; \xi_i^2)$ belonging to the segment that lies on coordinate ξ^2 , which is the interface of cells $I_{i,j}$ and $I_{i-1,j}$, the two WENO reconstructions and relations (24) and (25) lead to the definition of the pairs of values of dependent variables $h_{i-1/2,j}^{(n)-}, h_{i-1/2,j}^{(n)+}, q_{i-1/2,j}^{l(n)-}, q_{i-1/2,j}^{l(n)+}, \tau_{i-1/2,j}^{l(n)-}$ and $\tau_{i-1/2,j}^{l(n)+}$. Let $h_{i-1/2,j}^*, q_{i-1/2,j}^*$ e $\tau_{i-1/2,j}^*$ be the solution of the Riemann problem defined by the hyperbolic homogenous system of the Shallow Water Equations, written in the locally valid orthonormal basis, with initial data given by the pairs of point values of the unknown variables. The so-called exact solution of this Riemann problem is carried out by means of an iterative procedure [38]. Subsequently, by operating an inverse transformation of the reference system, the solution of the Riemann problem in contravariant components is evaluated. An analogous procedure is carried out for each one of the contour segments of the generic cell $I_{i,j}$. From the solution of local Riemann problems expressed in contravariant components, the point values of the variables involved in the calculation of the spatial integrals defining $\mathbf{L}(r^1, r^2, t)$ and $\mathbf{D}(h, r^1, r^2, t)$ in the relations (21) and (22), are evaluated.

In order to ensure numerical stability, the CFL-like criterion used by Titarev and Toro [36] in the framework of Cartesian coordinates is extended to the framework of generalized curvilinear coordinates. The cell Courant number, expressed in terms of variables defined in the generalized curvilinear system of reference, is given by

$$C_{i,j} = \max\left(\frac{w_{\xi_{i,j}^1}}{\Delta\xi_{i,j}^1}; \frac{w_{\xi_{i,j}^2}}{\Delta\xi_{i,j}^2}\right) \quad (26)$$

in which $w_{\xi_{i,j}^1}$ and $w_{\xi_{i,j}^2}$ are maximums of the characteristic speeds (related to the cell $I_{i,j}$ defined in the generalized curvilinear system of reference. The CFL-like stability criterion is obtained by assuming that the maximum value of $C_{i,j}$ amongst all the computational cells must be inferior than a threshold stability value C_s , that is

$$\max_{i,j}(C_{i,j}) \leq C_s \quad (27)$$

As stated by Titarev and Toro [36], for two-dimensional WENO schemes in Cartesian coordinates, the threshold stability value C_s is equal to 0.5. All the numerical simulations presented in this section are performed by fixing the constant $C_s = 0.4$.

5 Results and Discussion

In this section, the high-resolution Shallow Water Equations solver described above is verified against several benchmark test cases. The computed results are compared with the analytical solutions and previously published predictions.

5.1 Accuracy test

In this subsection the order of accuracy of the scheme on curvilinear grids is tested. A case test proposed by the working group on dam break modeling [22] and widely utilized to test numerical schemes for Shallow Water Equations (eg.[5,6,45]) is used. This test case consists in the simulation of a subcritical stationary flow over a Gaussian bump. The domain is a square (-15 m, 15 m)×(-15 m, 15 m). The bottom topography is defined by the Gaussian function,

$$H(x, y) = \frac{c_0}{\sigma\sqrt{2\pi}} \exp\left[-\frac{1}{2}\left(\frac{x-x_m}{\sigma}\right)^2\right] \quad (28)$$

with $c_0 = 1 \text{ m}^2$, $\sigma = 2 \text{ m}$ and $x_m = 15 \text{ m}$. A 2 m constant water level and a 0 discharge are the initial conditions. The boundary conditions are $hu_x = 4.42 \text{ m}^2/\text{s}$ and $hu_y = 0 \text{ m}^2/\text{s}$ (upstream) and $h=2 \text{ m}$ (downstream), where u_x and u_y are the Cartesian components of the depth averaged velocity vector \vec{u} . For this accuracy test case, the simulations are carried out on four curvilinear meshes (14×14,

28×28, 56×56, 112×112). The finest mesh (112×112) is generated by following the procedure proposed by Visbal and Gaitonde [42]. The 56×56 mesh is obtained by simply retaining one out of every two coordinate lines of the finest mesh. Such procedure is repeated in order to generate the 28×28 and 14×14 meshes. Fig. 1 shows the 56×56 grid used for the test case simulations. We compute the error in the discrete $L^1_{N \times M}$ norm for the water depth, defined as

$$L^1_{N \times M} = \sum_i^N \sum_j^M |h_{i,j} - \hat{h}_{i,j}| \sqrt{g_{i,j}} \Delta \xi^1 \Delta \xi^2 \quad (29)$$

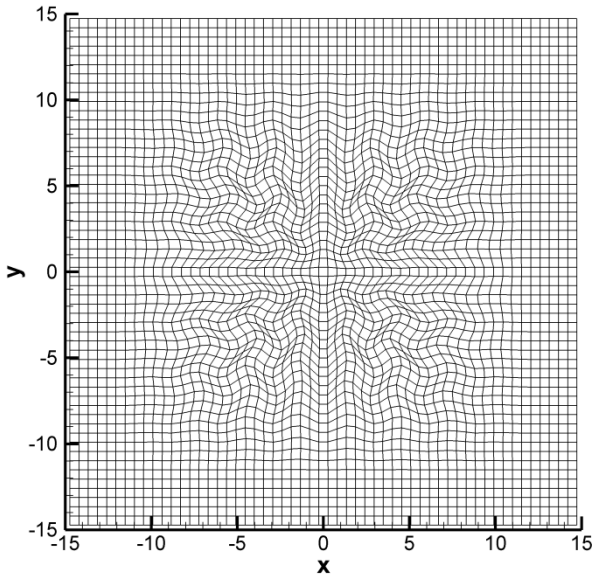


Figure 1: Steady flow over a Gaussian bump. 56×56 calculation grid.

in which N and M are the number of cells in the ξ^1 and ξ^2 directions, respectively, $\sqrt{g_{i,j}} \Delta \xi^1 \Delta \xi^2$ represents the area of the computational cell $I_{i,j}$ and $h_{i,j}$ and $\hat{h}_{i,j}$ are the numerical and the analytical point-values of the water depth, respectively. The spatial order of accuracy is evaluated by extending to the framework of generalized curvilinear coordinates, the procedure that many authors (e.g. Levy et al. [25], Titarev and Toro [36]) used in the framework of Cartesian coordinates; according to such procedure, the spatial order of accuracy of the numerical scheme is evaluated by using the equation which relates the $L^1_{N \times M}$ norm to the average spatial step size of the grid. Let $d_{N \times M}$ be the average spatial step size (measured in the Cartesian system of reference) of the $N \times M$ curvilinear grid, defined by the following expression

$$d_{N \times M} = \frac{\sum_i^N \sum_j^M [(\sqrt{g_{11}})_{i,j} \Delta \xi^1 + (\sqrt{g_{22}})_{i,j} \Delta \xi^2]}{N \cdot M} \quad (30)$$

in which $(\sqrt{g_{11}})_{i,j} \Delta \xi^1$ and $(\sqrt{g_{22}})_{i,j} \Delta \xi^2$ represent the side lengths of the cell $I_{i,j}$. The equation which relates the $L^1_{N \times M}$ norm to the average spatial step size $d_{N \times M}$ is given by

$$L^1_{N \times M} = b \cdot (d_{N \times M})^z \quad (31)$$

in which b is an arbitrary constant independent of N and of M , and z represents the spatial order of accuracy of the numerical scheme. Let us take a grid composed by $N_1 \times M_1$ cells and a grid composed by $N_2 \times M_2$ cells, with $N_2 = 2N_1$ and with $M_2 = 2M_1$, in which

$$d_{N_1 \times M_1} = 2 \cdot d_{N_2 \times M_2} \quad (32)$$

The ratio between the $L^1_{N \times M}$ norm and the $L^2_{N_2 \times M_2}$ norm gives, by Eqs. (31) and (33), the following expression for the evaluation of z

$$z = \log_2 \left(\frac{L^1_{N_1 \times M_1}}{L^1_{N_2 \times M_2}} \right) \quad (33)$$

With analogous procedures we compute the errors in the discrete L^1 norm and the order of accuracy for the depth-integrated Cartesian velocity components hu_x and hu_y . In Table 1 the accuracy analysis results obtained using the L^1 norm are reported. Table 1 shows that the fourth order spatial accuracy of the proposed scheme is achieved.

Table 1: Steady flow over a Gaussian bump. Accuracy analysis

Cells	h		hu_x		hu_y	
	L^1 norm	Ord.	L^1 norm	Ord.	L^1 norm	Ord.
14×14	2.12E+00		1.17E+01		1.16E+01	
28×28	1.14E-01	3.94	8.1E-01	3.85	8.37E-01	3.79
56×56	8.24E-03	4.06	4.5E-02	4.16	4.77E-02	4.13
112×112	4.1E-04	4.33	2.1E-03	4.42	2.34E-03	4.35

5.2 Symmetric channel constriction

The purpose of this test case is to verify the good resolution property of the proposed scheme for discontinuous solutions on highly distorted grids. The results obtained are compared with analytical solutions and alternative numerical solutions.

This test case, used by many authors [27,48], consists in the simulation of a super-critical flow in

a channel with wall constrictions. The channel is 40 m wide and 90 m long. Starting from $x=10$ m, the channel wall is symmetrically constricted from both sides with angle $\beta=5^\circ$ to the x direction. The initial and inflow conditions are the water depth $h=1$ m and Froude number $Fr=2.5$. Two grids are used for this test case: a 121×53 regular curvilinear grid, with nearly square-shaped calculation cells (see Fig. 2); a highly-distorted grid obtained by deforming the above-mentioned 121×53 regular grid (see Fig. 3). In Figs. 2 and 3 the results of the numerical simulation carried out by the model proposed in this paper, SWF scheme, on the regular grid and on the highly-distorted grid, respectively, are shown. In these figures the contour plots of the water depth with 16 uniformly spaced contour lines (from 1.05 to 1.8 m) are shown. From Figs. 2 and 3 it is evident that in both simulations shocks are nicely resolved, with results that are in very good agreement with those shown in [48], where a grid with a greater number of nodes is used. By comparing Figs. 2 and 3, it can be seen that there are no significant differences between results obtained on the regular grid and on the highly-distorted one.

In Fig. 4 the results of the numerical simulation carried out by the model proposed in Gallerano et al. [16], CWENO-SW scheme, is shown. The comparison between the Fig. 3 and 4 shows that the shock obtained by CWENO-SW scheme results less steep than the shock obtained by SWF scheme.

Numerical results obtained by simulations carried out by the SWF scheme and CWENO-SW scheme are compared with the analytical solution of this case, computed by adopting the procedure proposed by Ippen [23]. By comparing the aforementioned analytical solution and numerical results obtained by the SWF and CWENO-SW scheme, L^1 norms of the error in h and in the modulus of the depth-averaged velocity vector $V = |\bar{u}|$ are computed; L^1 norms are shown in Table 2. From this table it is evident that, even in the presence of discontinuities in the solution, the L^1 norm of the error computed with SWF scheme on the highly-distorted grid is less than 6% greater to the L^1 norm of the error computed with SWF scheme on the regular grid. Table 2 also shows that the norm of the error L^1 computed with the scheme proposed in Gallerano et al [16] (CWENO-SW scheme) is greater than the norm of the error L^1 computed with SWF.

By the comparison between the results obtained, it is evident that the presence of highly-distorted cells does not compromise the proposed scheme's capability to integrate the Shallow Water Equations

whose solutions are characterized by discontinuities and shocks.

Table 2: Symmetric channel constriction. Comparison between results obtained on a regular grid and a highly-distorted grid.

	L^1 norm (h)	L^1 norm (V)
Regular grid (SWF scheme)	4.23E+01	5.57E+01
Highly-distorted grid (SWF scheme)	4.48E+01	5.91E+01
Highly-distorted grid (CWENO-SW scheme)	5.15E+01	6.27E+01

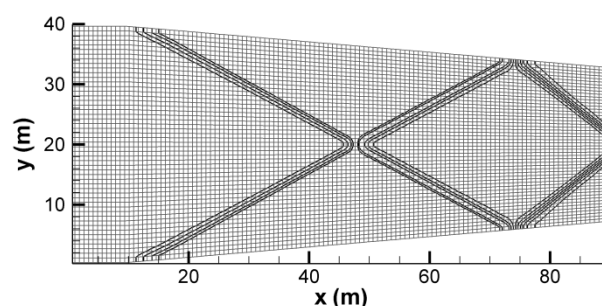


Figure 2: Symmetric channel constriction. Contour plot of the water depth. 15 uniformly spaced contour lines from 1.05 m to 1.8 m. Simulation carried out by means of the SWF scheme on regular grid.

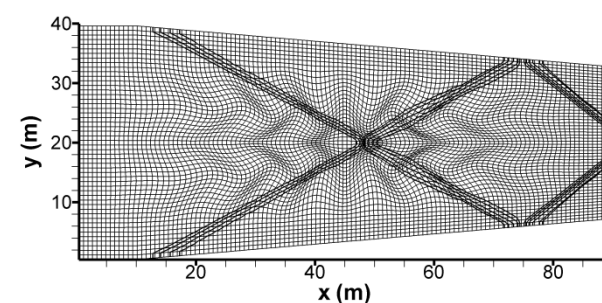


Figure 3: Symmetric channel constriction. Contour plot of the water depth. 15 uniformly spaced contour lines from 1.05 m to 1.8 m. Simulation carried out by means of the SWF scheme on highly-distorted grid.

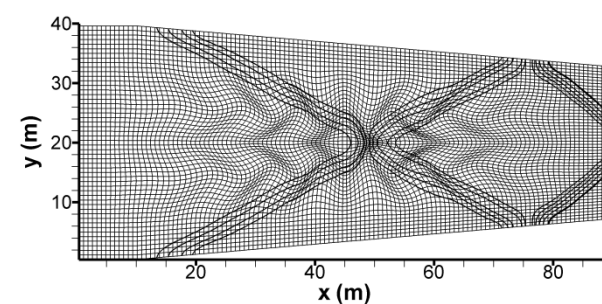


Figure 4: Symmetric channel constriction. Contour plot of the water depth. 15 uniformly spaced contour lines from 1.05 m to 1.8 m. Simulation carried out by means of the CWENO-SW scheme on highly-distorted grid.

5.3 Freestream preservation property test

In numerical methods in which the numerical approximation of derivatives of uniform physical quantities do not vanish, freestream conditions are not preserved. In other words, the freestream preservation properties of a scheme are achieved when a uniform field remains uniform and it is not affected by mesh irregularities. In this subsection the capability of the proposed numerical scheme to preserve the freestream condition over highly-distorted grids is tested. A test case consisting in the simulation of a frictionless uniform flow in a square domain with flat bottom is used. The domain on which the test is carried out (a $30 \times 30 \text{ m}^2$ square) and the boundary conditions ($hu_x=4.42 \text{ m}^2/\text{s}$ and $hu_y=0 \text{ m}^2/\text{s}$ upstream; $h=2 \text{ m}$ downstream) are equal to those used for the accuracy test. Initial conditions consist in a constant value of the water depth $h=2 \text{ m}$ and depth-integrated Cartesian velocity component values equal to $hu_x=4.42 \text{ m}^2/\text{s}$ and $hu_y=0 \text{ m}^2/\text{s}$. The analytical solution of this test case consists in the maintaining of the initial conditions. The highly-distorted mesh used for this test case is the same 56×56 mesh used for the accuracy test, shown in Fig. 1. Let us indicate with SWNF the numerical scheme obtained by applying the numerical integration procedure presented in Section 4 to motion Eqs. (7) and (9). Let us indicate with SWF the scheme set up by applying the same numerical integration procedure to equations obtained by adding to the right-hand side of (7) and (9) the terms (16)

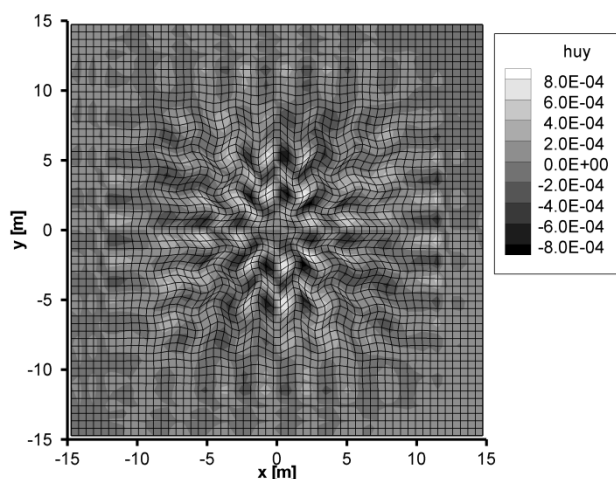


Figure 5: Freestream preservation property test. Contour plots of the hu_y component obtained by means of the SWNF scheme.

Table 3: Freestream preservation property test. Comparison between results obtained by the SWF and SWNF schemes. L^1 norm of the error in the water depth h and the depth-integrated cartesian velocity component, hu_x and hu_y , at instant $t=50\text{s}$.

	L^1 norm (h)	L^1 norm (hu_x)	L^1 norm (hu_y)
SWF	3.3E-16	6.4E-14	6.2E-14
SWNF	2.6E-02	2.9E-01	5.7E-02

and (17), respectively, which are introduced in order to correct the errors due to the failure to satisfy the metric identities. Fig. 5 shows the results of this case simulation carried out by means of the SWNF scheme; in this figure contour plots of the modulus of hu_y at time $t = 50 \text{ s}$ are shown. Since in this test case hu_y should be null, the numerical values of hu_y shown in Fig. 5 represent a measure of the error produced by the numerical simulation carried out by the SWNF scheme. From Fig. 5 it is possible to highlight and quantify the errors arising from the numerical approximation of metric terms. As Fig. 5 shows, the modulus of hu_y (which should be null) is as great as the distortion of the grid. The failure to satisfy of the metric identities produces significant numerical errors also in the hu_x component and in the water depth h . In Table 3 the L^1 norm of the error in h , hu_x and hu_y at instant $t = 50 \text{ s}$, obtained by carrying out this test case by the SWNF and SWF schemes, are compared.

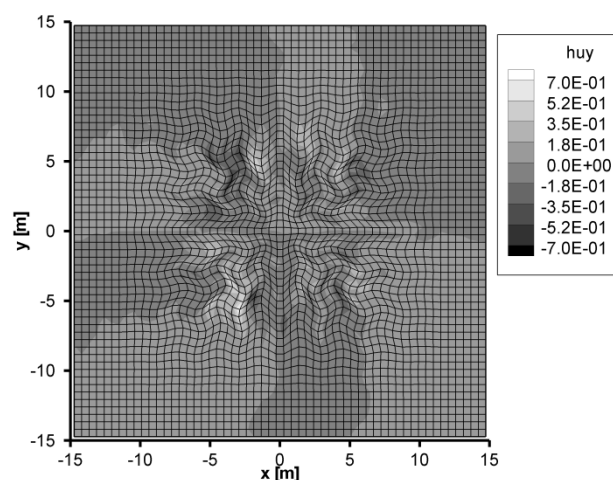


Figure 6: Freestream preservation property test. Contour plots of the hu_y component obtained by means of the SWCH scheme.

Table 4: Freestream preservation property test. Comparison between results obtained by the SWF and SWCH schemes. L^1 norm of the error in the water depth h and the depth-integrated cartesian velocity component, hu_x and hu_y , at instant $t=50s$.

	L^1 norm (h)	L^1 norm (hu_x)	L^1 norm (hu_y)
SWF	3.3E-16	6.4E-14	6.2E-14
SWCH	3.2E-00	4.3E+01	7.2E+01

From the results shown in Table 3 it can be seen that, in the case of a uniform flow on a highly-distorted grid, the numerical scheme in which the terms that correct the errors associated with the metric identities are present is capable of reducing numerical errors in h , hu_x and hu_y to machine precision. In order to demonstrate that numerical discretization of the Christoffel symbols can reduce the numerical accuracy and can corrupt the preservation of freestream conditions, the numerical procedure presented in Section 4 is applied to the integral form of the contravariant Shallow Water Equations in which Christoffel symbols are present; the scheme thus obtained is called SWCH. Fig. 6 shows the results of the simulation of the freestream preservation property test case carried out by means of the SWCH scheme; in this figure contour plots of the modulus of hu_y at time $t = 50$ s are shown. As stated before, in this test case hu_y should be null, hence the numerical values of hu_y shown in Fig. 6 represent a measure of the error produced in the numerical simulation by the presence of the Christoffel symbols. Fig. 6 shows that the modulus of hu_y is greater in zones in which the coordinate lines are more curved. In such zones, the rate of change of the local base vectors are higher, hence the values of Christoffel symbols and errors related to the discretization of the aforementioned symbols are higher. In Table 4 the L^1 norm of the error in h , hu_x and hu_y at instant $t = 50$ s, obtained by carrying out this test case by the SWF and SWCH schemes, are compared. The norms of the errors related to the simulation carried out by the SWF scheme are of the same order of magnitude of machine precision, while the norms of the errors produced by the SWCH scheme are significative.

The comparison between results obtained by means of the SWF and SWCH schemes highlights that on highly-distorted grids numerical errors due to discretization of Christoffel symbols produce spurious oscillations that impede the simulation of a steady-state uniform flow with flat bottom, whereas the simulation carried out with the SWF scheme does not alter the initial steady-state.

6 Conclusion

An Upwind WENO scheme in which an exact Riemann solver is involved has been developed for the numerical integration of the contravariant Shallow Water Equations. An integral expression of the Shallow Water Equations in a contravariant formulation in which Christoffel symbols are absent has been presented. A procedure has been proposed in order to correct the effects produced by the spurious source terms related to the difficulties of numerically satisfying the metric identities; such procedure allows the proposed numerical scheme to preserve the freestream conditions on highly-distorted grids. It has been demonstrated that the numerical scheme obtained by discretizing the contravariant Shallow Water Equations in which Christoffel symbols are present produces spurious oscillations that do not permit the simulation of steady flows on highly-distorted grids. The proposed numerical scheme related to the contravariant Shallow Water Equations in which Christoffel symbols are absent is 4th order accurate and possesses good non-oscillatory properties and good shock-capturing properties on highly-distorted grids.

References:

- [1] Aris R, *Vector Tensor, and the Basic Equations of Fluid Mechanics*, New York, NY, USA: Dover; 1989.
- [2] Arminjion P. St-Cyr A, Nessyahu-Tadmor-type central finite volume methods without predictor for 3D Cartesian and unstructured tetrahedral grids, *App Numer Math*, Vol.46, No.2, 2003, pp. 135-55.
- [3] Brocchini M. Bernetti R. Mancinelli A. Albertini G, An efficient solver for nearshore flows based on the WAF method, *Coast Eng*; Vol.43, No.2, 2001, pp.105-29.
- [4] Cai X. Ladeinde F, Performance of WENO scheme in generalized curvilinear coordinate systems, In: 46th AIAA areospace sciences meeting and exhibith, Reno (Nevada), 2008, pp.1-16.
- [5] Caleffi V, Valiani A, Bernini A, Foruth-order balanced source term treatment in central WENO schemes for shallow water equations. *J Comput Phys*, Vol.218, No.1, 2006, pp. 228-45.
- [6] Canestrelli A. Siviglia A. Dumbser M. Toro E, Well-balanced high-order centred schemes for non-conservative hyperbolic systems. Applications to shallow water equations with

- fixed and mobile bed, *Adv Water Resour*, Vol.32, No.6, 2009, pp.834-44.
- [7] Capdeville G, A central WENO scheme for solving hyperbolic conservations laws on non-uniform meshes, *J Comput Phys*, Vol.227, No.5, 2008, pp.2977-3014.
- [8] Casonato M. Gallerano F, A finite difference self-adaptive mesh solution of flow in a sedimentation tank. *Int J for Num Meth in fluids*, Vol.10, No.6, 1990, pp. 697-711.
- [9] Cioffi F. Gallerano F. Napoli E, Tree dimensional numerical simulation of wind driven flows in closed channel and basins, *Journal of Hydraulic Research*, Vol. 43, No 3, 2005, pp.290-301.
- [10] Esfahanian V. Ashrafi K, Equation-Free/Galerkin-Free reduced-order modeling of the shallow water equations based on proper orthogonal decomposition, *J of Fluids Engineering*, ASME, Vol.131, No.7, 2009.
- [11] Font JA, Numerical Hydrodynamics in General Relativity, *Living Rev Relativ*, Vol.3, No.2, 2000, pp. 200.
- [12] Gallerano F. Cannata G, Form invariance and frame indifference of closure relations in LES, *WSEAS transaction on applied and theoretical mechanics*, Vol.1, No.1, 2006, pp47-54.
- [13] Gallerano F. Cannata G. Melilla L, New closure relations for the balance equations of the SGS viscous dissipation in LES, *WSEAS transaction on fluid mechanics*, Vol.1, No.6, 2006, pp.558-565.
- [14] Gallerano F. Cannata G. Melilla L, The dynamic procedure for closure relations in the equation of the filtered concentration of suspended solid particles, *WSEAS transaction on fluid mechanics*, Vol.1, No.6, 2006, pp. 738-744.
- [15] Cannata G. Lasaponara F. Gallerano F, A contravariant formulation of non-linear shallow water equations, *Recent advances in applied mathematics, modeling and simulation*, North Atlantic university union, ASM14, 2014, WSEAS press, pp. 299-306.
- [16] Gallerano F. Cannata G, Central WENO schemes for the integral form of contravariant shallow water equations. *Int J Numer Meth Fl*, Vol.67, No.8, 2011, pp939-59.
- [17] Gallerano F. Cannata G, Compatibility of reservoir sediment flushing and river protection, *Journal of Hydraulic Engineering*, Vol. 137, No 10, 2011, pp.1111-1125.
- [18] Gallerano F. Cannata G. Tamburrino M, Upwind WENO scheme for shallow water equations in contravariant formulation, *Comput. Fluids*, Vol.62, 2012, pp.1-12.
- [19] Gallerano F. Cannata G. Villani M, An integral contravariant formulation of the fully non-linear Boussinesq equations, *Coastal Eng*, Vol.83, 2014, pp.119-136.
- [20] Gallerano F. Napoli E, A dynamic subgrid-scale tensorial eddy viscosity model, *Continuum Mechanics and Thermodynamics*, Vol. 11, No 1, 1999, pp.1-14.
- [21] Gallerano F. Pasero E. Cannata G, A dynamic two-equation sub grid scale model, *Continuum Mechanics and Thermodynamics*, Vol. 17, 2005, No. 2, pp. 101-123.
- [22] Goutal N. Maurel F, In: Proceedings of the Second Workshop on Dam-Break wave simulations, *Thec. Rep*, Vol.42, No.16, 1997, pp.97.
- [23] Ippen AT, High-velocity flow in open channels: A symposium, *Trans ASCE*, Vol.116, 1951, pp.265-95.
- [24] Jiang GS. Shu CW, Efficient Implementation of Weighted ENO schemes, *J Comput Phys*, Vol.126, No.1, 1996, pp.202-28.
- [25] Levy D. Puppo G. Russo G, A Fourth-order WENO scheme for multidimensional hyperbolic systems of conservations laws, *SIAM J Sci Comput*, Vol.24, No.2, 2002, pp.480-506.
- [26] Liang Q, Simulation of Shallow Flows in Nonuniform Open Channels, *J of Fluids Engineering*, ASME, Vol.130, No.1, 2008.
- [27] Liska R. Wendroff B, Two-dimensional shallow water equations by composite schemes, *Int J Numer Meth Fl*, Vol.30, No.4, 1999, pp.461-79.
- [28] Liu X, Osher S. Chan T. Weighted Essentially Non-oscillatory Schemes, *J Comput Phys*, Vol.115, No.1, 1994, pp.200-12.
- [29] Maciel M, "Frink, Parikh and Pirzadeh and Liou and Steffen Jr. TVD Algorithms and Implicit Formulations Applied to the Euler Equations in 2D, *WSEAS transaction on fluid mechanics*, Vol.7, No.4, 2012, pp. 129-145.
- [30] Marti JM. Muller E, Numerical Hydrodynamics in Special Relativity, *Living Rev Relativ*, 1999.
- [31] Nonomura T. Iizuka N. Fujii K, Freestream and vortex preservation properties of high order WENO and WCNS on curvilinear grids, *Comput Fluids*, Vol.39, No. 2, 2010, pp.197-214.
- [32] Pan CH. Lin BY. Mao XZ, Case Study: Numerical Modeling of the Tidal Bore on the Qiantang River. China, *J Hydraul Eng*; Vol.133, No.2, 2007, pp.130-8.

- [33] Rosmanith J. Bale DS. LeVeque RJ, A wave propagation algorithm for hyperbolic systems on curved manifolds, *J Comput Phys*, Vol.199, No.2, 2004, pp.631-62.
- [34] Selescu R, The velocity Potential PDE in an Orthogonal Curvilinear Coordinate System, *WSEAS transaction on fluid mechanics*, Vol.9, 2014, pp. 58-77.
- [35] Spiteri RJ. Ruuth SJ, A New Class of Optimal High-Order Strong-Stability-Preserving Time Discretization methods, *SIAM J Numer Anal*, Vol.40, No.2, 2002, pp.469-91.
- [36] Titarev V. Toro E, Finite Volume WENO schemes for three-dimensional conservation laws. *J Comput Phys*, Vol.201, No.1, 2004, pp.238-60.
- [37] Titarev V. Drikakis D, Uniformly high-order schemes on arbitrary unstructured meshes for advection-diffusion equations, *Computer & Fluids*, Vol.46, No.1, 2011, pp.467-71.
- [38] Toro E, *Shock-Capturing Methods for Free-Surface Shallow Flows*. Manchester: John Wiley and Sons, Inc. 2001.
- [39] Triki A, A Finite Element Solution of the Unidimensional Shallow-Water Equation, *J of Fluids Engineering*, ASME, Vol.80, No.2, 2013.
- [40] Thompson JF. Warsi ZUA. Mastin CW, *Numerical grid generation: foundations and applications*. New York, NY, USA: Elsevier North-Holland, Inc.; 1995. ISBN 0-444-00985-X.
- [41] Vinokur M, An analysis of finite-difference and finite-volume formulations of conservation laws, *J Comput Phys*, Vol.81, 1989, pp.1-52.
- [42] Visbal M. Gaitonde D, On the Use of Higher – Order Finite-Difference Schemes on Curvilinear and Deforming Meshes, *J Comput Phys*, Vol.181, No.1, 2002, pp.155-85.
- [43] Wei Y. Mao XZ. Cheung KF, Well-Balanced Finite-Volume Model for Long-Wave Runup. *J Waterw Port Coast Ocean Eng*, Vol.132, No.2, 2006, pp.114-24.
- [44] Wesseling P. Segal A. Kassels CGM, Computing flows on general three-dimensional Nonsmooth staggered grids, *J Comput Phys*, Vol.149, 1999, pp.333-62.
- [45] Xing Y. Shu CW, High order well-balanced finite volume WENO schemes and discontinuous Galerkin methods for a class of hyperbolic systems with source terms. *J Comput Phys*, Vol.214, No.2, 2006, pp.567-98.
- [46] Xu H. Zhang C, Numerical calculations of laminar flows using contravariant velocity fluxes, *Comput Fluids*, Vol.29, No. 2, 2000, pp.149-77.
- [47] Yang HQ. Habchi SD. Przekwas AJ, General Strong Conservation Formulation of Navier-Stokes Equations in Nonorthogonal Curvilinear Coordinates. *AIAA J*, Vol.5, No.32, 1994, pp.936-41.
- [48] Zienkiewicz OC. Ortiz P, A split-characteristic based finite element model for the shallow water equations, *Int J Numer Meth Fl*, Vol.20, No.8-9, 1995, pp.1061-80.